Journal of Population Therapeutics & Clinical Pharmacology

RESEARCH ARTICLE

DOI: 10.53555/jptcp.v30i18.3411

AN OVERVIEW ON SILICA NANOPARTICLES ABILITY TO INDUCE AUTOPHAGY IN HUMAN LUNG ADENOCARCINOMA A549 EXAMINED WITH ULTRA-STRUCTURE ANALYSIS

Fawziah A. AL-Salmi[1*]

[1*]Department of Biology, Faculty of Sciences, Taif University, Taif, Saudi Arabia

***Corresponding Author:** Fawziah A. AL-Salmi
*Email: f.alsalmi@tu.edu.sa

Abstract

Metal nanoparticles are potential agents that cause autophagy dysfunction. Silica nanoparticles (SiNPs) can induce autophagy. Hence, the goal of this study is to provide evidence of the ability of silica nanoparticles to induce autophagy-associated apoptosis. In this report, silica nanoparticles exhibited dose-dependent cytotoxicity in lung adenocarcinoma A549 cells. Multiple assays verified that the activity of silica nanoparticles to induce autophagy blocked the autophagic flux at 50µg/ml. Furthermore, SiNPs impaired lysosomal function by damaging lysosomal ultrastructures. The results revealed that silica nanoparticles activated apoptosis with 26.39% and arrested the cell cycle at S phase due to an increase in the percentage of cells at S with 10 percent as compared with the negative control. Furthermore, the caspase 3 assay indicated that the activity of silica nanoparticles to induce apoptosis throughout the caspase cascades was evaluated by inducing oxidative stress (MDA), which is considered a lipid peroxidation marker. The rt-Pcr results showed down-regulation of LC3, while beclin 1 showed overexpression. Both LC3 and beclin 1 are autophagic genes that regulate the autophagy process. The immunohistochemistry showed a weaker Beclin 1. Transmission electron microscopy showed autophagosomes that are considered the benchmark for autophagy studies; the number of double-membrane autophagosomes and single-membrane autolysosomes was obviously observed in SiNP-treated A549. The current study provides a potential mechanism for autophagy dysfunction induced by silica nanoparticles in A549 cells.

Keywords: Beclin-1, LC3, caspase 3, silica nanoparticles, autophagy, apoptosis, human lung adenocarcinoma A549, ultra-structure analysis.

Introduction

Lung cancer is classified as the most aggressive cancer type among men and women in the world. It includes two categories: non-small-cell lung carcinoma (NSCLC) and small-cell lung carcinoma (SCLC) [1]. The percentage of NSCLC cases is approximately 85% of all cases. The difficulty of lung cancer is its low survival rate (5%) [2]. Scientists are now interested in it as a new approach to cancer therapy. Autophagy plays a central role in tumorigenesis, development, and sensitivity to chemoradiotherapy [3–5]. Autophagy has two functions: firstly, prevention of cancer invasion and inhibition of cancer growth; and secondly, it is a response to provide a difficult environment to restrict and suppress cancer progression [6]. Also, autophagy can activate the self-degradation of cancer cells, leading to their death [6]. Autophagy is a catabolic process that ages cellular

organelles, lysosomes, and defective cytoplasmic components. It is divided into three classes: macroautophagy, microautophagy, and chaperone-mediated autophagy [7–8]. But the major autophagic process is macroautophagy [9]. Autophagy depends on proteins such as Beclin 1. It is a 60-kDa protein of 450 amino acids, and it includes three functional domains [10], which have multiple roles in tumorigenesis and also enter development, endocytosis, response to stress, aging, and cell death. But the basic function of beclin 1 is the regulation of the autophagy process via its phosphorylation. It enters the initial phase of autophagolysosome formation [11]. The integration of nanotechnology with biological fields in fabrication and/or application created a new era called the nanobiotechnology stage. Last decade, the combination of nanotechnology tools in the biological field reflected a huge advance and development in different applications, especially in medical science [12]. Moreover, the use of nanomaterials is becoming more popular in cancer detection and treatment. It is divided into different dimensions (1D and 2D) [13]. The benefits of using nanomaterials have been to decrease adverse effects as well as minimize therapy resistance [14-15].Currently, silica nanoparticles are more popular in biomedical applications because of their benefits, such as biocompatibility and colloidal stability. These interesting properties encourage the researchers to utilize them in different applications such as bio-sensing [16], bone repair [17], and diagnostics and drug delivery [18–19]. In this study, silica nanoparticles were prepared using Aspergillus *niger* as a novel approach to synthesising nanomaterials with green methods, then prepared silica nanoparticles on the lung adenocarcinoma A549 by cell viability assay, apoptosis assay, and studied the effect of the Si-NPs on autophagy genes LC3 and beclin-1 and apoptosis genes caspase3 using RT-PCR, immunohistochemistry, and observed the morphemically changed in the cell during treatment with silica nanoparticles using transmission electron microscopy.

Materials and methods

Green synthesis of silica nanoparticles

In this work, silica nanoparticles (SiNPs) were synthesized using a green method throughout microorganisms. In details, the fungal Aspergillus *niger* (RCMB 002F008) was inoculated in fungal culture (MGYP broth media). Then, 500 ppm of Na_2 SiO_3 dissolved in the fungal culture and adjusted the pH at 6.2± 0.2. The culture was growing in aerobically agitated at 28°C at speed 200 rpm for 5 days. The sterile filtration and re-suspension in sterile deionized distilled water were achieved. The supernatant was kept at ± 4.0 ℃.

Characterization of silica nanoparticle

Silica nanoparticles was characterized using physiochemical techniques such as Fourier transformed infrared (FT-IR) spectrum via the Nicolet 6700 apparatus (Thermo Scientific Inc., USA), XRD (D8 Advance X-ray diffractometer, Bruker, Germany), the morphology of silica nanoparticles were tested by Transmission Electron microscopy (TEM, JSM- 2100F, JEOL Inc., Tokyo, Japan), Scanning Electron microscopy (SEM, JSM-690, JEOL Inc.,Tokyo, Japan).Particle size, polydispersity index (PDI) and zeta potential were determined by a Malvern Zetasizern 3000 HSA (Malvern, Worcs, UK). The prepared silica nanoparticles were diluted to a suitable concentration (10-fold dilution) with distilled DMEM medium, and the samples were tested immediately. Experiments were conducted in triplicate.

Cell lines

Human lung adenocarcinoma (A549) has been obtained from American Type Culture Collection. The preservation of cells was achieved in a ninety-five percent air and five percent carbon dioxide humidified atmosphere at 37°C. Ten percent fetal bovine serum and one percent polystyrene were added to Dulbecco's Modified Eagle medium in purpose of subculturing process and experimentation.

Cell viability assays

A549 cell line ability of being viable has been evaluated utilizing MTT test as stated before by Mossman [14] with a few adjustments. In brief, 1 × 10 cells/well have been seeded in 96-well plates and treated with silica nanoparticles at the concentrations of 100 μg/ ml , 50 μg/ ml, 25 μg/ ml, 12.5

μg/ ml, 6.25 μg/ ml and non-treated as negative control for 24 hour. At the end of exposure, culture medium was discharged from each well to avoid interference of silica nanoparticles , then replaced with fresh medium including (0.5 mg/mL) of MTT solution in an amount equal to 10% of the culture volume and incubated for 4 hour at 37°C until a purple-colored formazan product developed. The formazan product was dissolved in acidified isopropanol. In addition to that, a one hundered milliliter of supernatant was putted into the other wells of a 96- well plate, and the determination of absorbance has been done at 570 nm by a microplate reader.

Analysis of cellular DNA

A549 cells (1×10^6) were planted into T520 flasks and then subjected to varying concentrations of silica nanoparticles at 70-80% confluence. Media was aspirated after 24 hours and with aid of 0.25% trypsin cells have been harvested then fixed in ice cold ethanol that having a concentration of 70% at −20°C for 30 min. Pellets have been picked up and washed with phosphate buffered saline then re-suspended in 500 μl phosphate buffered saline which includes 20 μl RNAse with a concentration of 5 mg/ml and stained with 10 μl Propidium iodide with 1 mg/ml concentration for 30 min at 37°C. Viable cells were quantified using flowcytometry.

Apoptosis assay

A549 cells (1×10^6) have been placed in T75 flasks and at 70-80% confluence exposed to treatment with variable concentrations of silica nanoparticles. Following 24 hours, the media was underwent through aspiration process and using 0.25% trypsin the cells were harvested and fixed by 70% ice cold ethanol at temperature of −20°C for nearly 30 min. After that, The Pellets were gathered and underwent through washing using phosphate buffered saline with 0.5 ml binding buffer containing FITC-Annexin V and Propidium iodide and left at 25°C temperature in the dark for 30 min.

Oxidative stress and Antioxidant biomarkers

Human lung adenocarcinoma A549 was obtained from ATCC , USA . In brief, 1 x 10^4 cells/well were seeded in 96-well plates and exposed for 24 hours to 50 μg/ml of silica nanoparticles. Whole cell lysate was prepared after 24 hours of cell culture for oxidative and anti-oxidative assays. A549 cells were tested for lipid peroxidation using thiobarbituric acid reactive substances as a marker through utilization of procedure that presented by Ohkawa et al. (1979) [12] and the level of nitrate/nitrite ratio has been measured by execution of the method outlined by Green et al. (1982) [12].

Caspase-3 fluorometric assay

Caspase-3 enzyme activity was measured using standard fluorometric microplates [14]. In short, cells were cultured in a 96-well plate and have an exposure to silica nanoparticles treatment with a concentration of 50 μg/ ml for 24 hour. After completion of the duration of exposure, in order to prepare cell lysate, the cells were underwent harvesting in ice-cold phosphate buffer saline. In addition to that, for the sake of making a reaction mixture, 30 mL of cell lysate, 20 mL of Ac-DEVD-pNA which is considered to be caspase-3 substrate and 150 mL of protease reaction buffer were added together and incubated for 15 min. A 5 minutes intervals for a total of 15 minutes were used to measure the fluorescence of the reaction mixture at excitation and emission wavelengths of 430/535 nm utilizing an ELISA reader apparatus. In order to calculate caspase-3 activity in terms of pmol AFC released/minute/mg protein, 7- amido-4-tri-fluoromethyl coumarin standard ranging from 5m to 15 mM was prepared, and its fluorescence has been recorded.

RNA isolation and qRT-PCR

The A549 cells were culturing has been done in six-well plates and treated with silica nanoparticles those have a concentration of 100 mg/ml and kept for 24 hour. When end of exposure process is achieved and regarding to the manufacturer's directions, all of the RNA has been extracted through utilization of RNeasy mini Kit (Qiagen, Valencia, CA, USA). The resulted RNA from extraction has been measured utilizing Nanodrop 8000 spectrophotometer (Thermo-Scientific, Wilmington, DE), QuantiTect SYBR Green PCR Kit was used to evaluate the mRNA expression of the genes that were identified (Qiagen, USA). For normalization, Ct values for the housekeeping gene GAPDH were used. To estimate fold changes in the expression of the identified genes, the

following PCR conditions were used: 94°C for 5 min, 40 cycles (94°C for 30 sec, 60°C for 30 sec, and 72°C for 45 sec). To estimate the relative gene expression suggested by fold variations in measured mRNA, delta-delta Ct equations have been applied.

Table 1. the list the primers used in the RT-PCR assay

Primer	**Sequence (5'-3')**
LC3	F: TGCAGATTATGCGGATCAAACC
	R: GCATTCACATTTGTTGTGCTGTAG
Beclin 1	F: CTGGACACTCAGCTCAACGTCA
	R: CTCTAGTGCCAGCTCCTTTAGC
GAPDH	F: GTCTCCTCTGACTTCAACAGCG
	R: ACCACCCTGTTGCTGTAGCCAA

Immunohistochemistry

The sections that were embedded in paraffin were deparaffinized and then immunohistochemically stained for Beclin 1 antibody (Cell Signal Technology). For a total of 20 minutes, the sections were microwaved in a buffer of 10mM sodium citrate (pH 6.0) at 10 minute intervals. The sections were incubated in a 3.0 % hydrogen peroxide solution for 20 minutes at room temperature to block endogenous peroxidase activity. The sections were incubated overnight at 4 °C with the primary Beclin 1 (1:200) antibody after washing in phosphate buffered saline. After washing the sections with phosphate buffered saline, they were incubated with biotinylated secondary antibody for 30 minutes, then an incubation through utilization of streptavidin–biotin–peroxidase complex, a solution of 3,3′-diaminobenzidine which includes hydrogen peroxide with 1.0 % and lightly counterstained using Harris hematoxylin. All images have undergone analysis using Image Pro Plus software. The Intensity of staining and the non-tissue area that covered by whitespace were recorded for each image (2 to 3 images per slide).

Transmission electron microscope to reveal Ultrastructure of A549

The cells have undergone through treatment by two concentrations of silica nanoparticles which are 25 and 50 μg/ml for a period of 24 hours. Following the treatment, cells were assembled and fixed in ice-cold glutaraldehyde (2.5%) for one hour after being washed using phosphate buffered saline. For three times, the cells have been washed with phosphate buffered saline for nearly 15 min. In addition to that, the cells were fixed in Osmium tetroxide (1%) for one hour, after that they were stained with uranyl acetate (2%) for 30 min at 25 $^{\circ}$C. Serial dilutions using ethanol with different concentraions for 15 minutes each (50, 70, and 90%) have been made and the cells were dehydrated, subsequent steps were included putting the cells for 20 minutes in ethanol (100%) then 20 minutes in acetone (100%). Furthermore, the cells were embedded in Epoxy Embedding Medium. Ultrathin sections which have the thickness of 120 nm were acquired and underwent statining using uranyl acetate (2%) for a duration of 20 min and staining using lead citrate for 5 min, then examination has been done utilizing Transmission Electron Microscope (TEM) with accelerating voltages of 15 kV and 200 kV.

Statistical analysis through measuring standard deviation

The mean standard deviation of triplicate experiments was used to express the statistical analysis. Student's t-test analysis has been executed to obtain the results of two sample comparisons of means. All the processes have been done utilizing SPSS 17.0 software and $P < 0.05$ was assessed as a statistically significant difference [13].

Results

Characterization of silica nanoparticle

This work's aim was to examine the anticancer effect of synthesized silica nanoparticles. As being noticed in figure 1, Fourier transformed infrared spectra of the Si-NPs; there is an existence of a

band at 3,429 cm-1 that resulted from the hydroxyl group of a water molecule on the nanoparticles surface. Another band existed at 1,033 cm-1 associated to the OH bend in Si-NPs. Furthermore, a strong band at 553 cm-1 is related to Si. The synthesized silver nanoparticles used in this study were characterized by X-ray diffraction (XRD), (TEM), The XRD patterns for synthesized silica nanoparticles demonstrated showed that main characteristic diffraction peaks for si were observed at 2 Θ = 35.634°, which are assigned to 111. It was matched with the standard silver diffraction pattern according to the Joint Committee on Powder Diffraction standards (JCPDS-16-1157 Diff. card), as Figure 2 showed. As figure 3 displayed, the hydrodynamic size and zeta potential were measured at 24 h in serum-free DMEM as the following: the hydrodynamic size was 102 nm with the zeta potential equal 37 mV with PDI 0.10. These data indicated that the prepared Si-NPs possessed favorable stability and monodispersity in both stock solution and culture medium. As figures 4 The SEM images depicted the spherical shapes of silica nanoparticles with smooth surface. The TEM image displayed the silica nanoparticle with particle sizes of 35 nm, as shown in Figure 5, emphasizing the fabrication of silica nanoparticles in a regular shape.

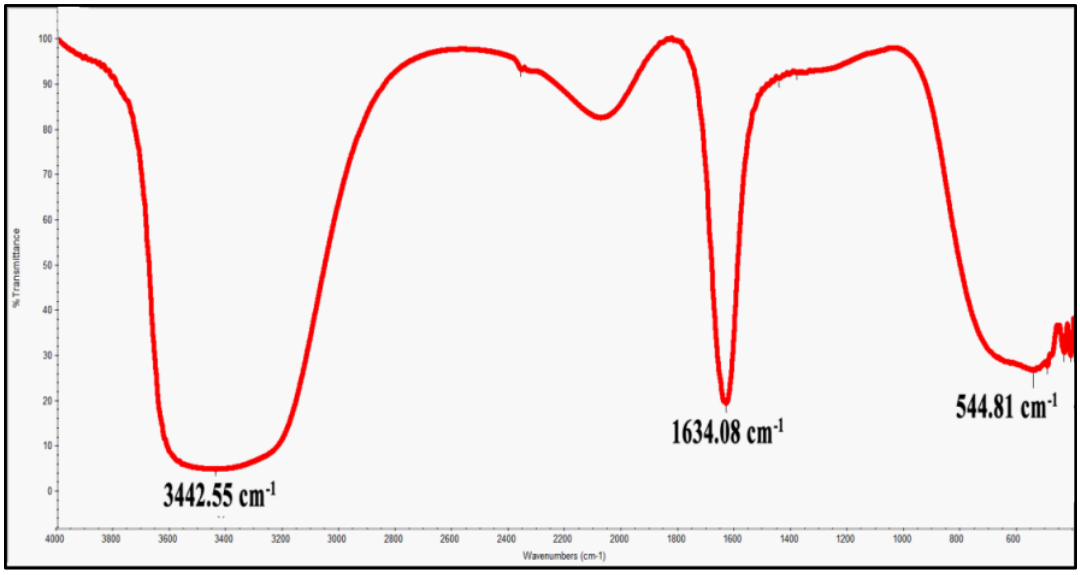

Figure 1: FT-IR of silica nanoparticles synthesized using green methods

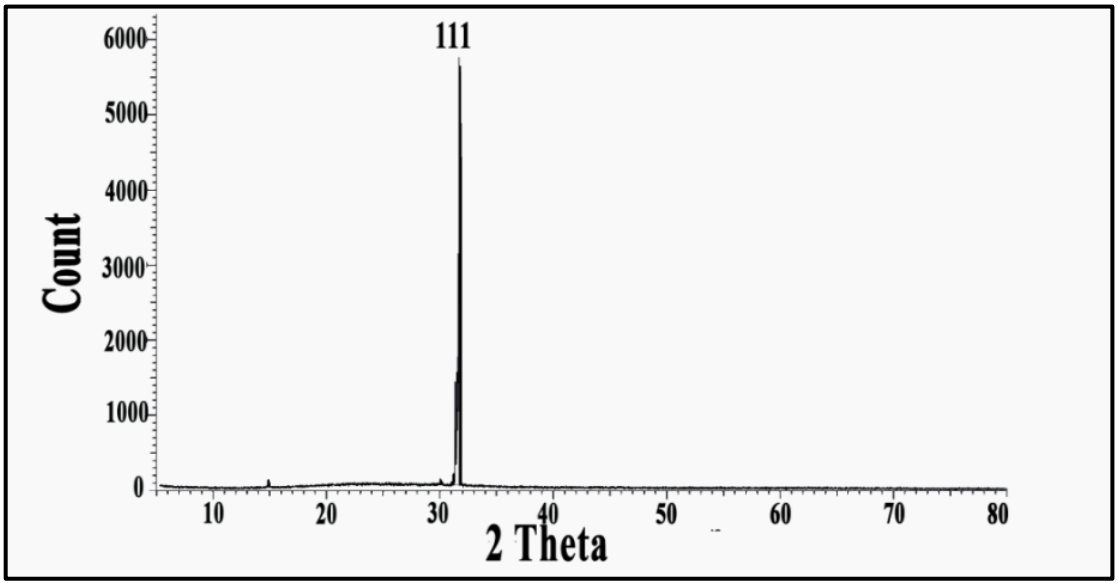

Figure 2: XRD of silica nanoparticles synthesized using green methods

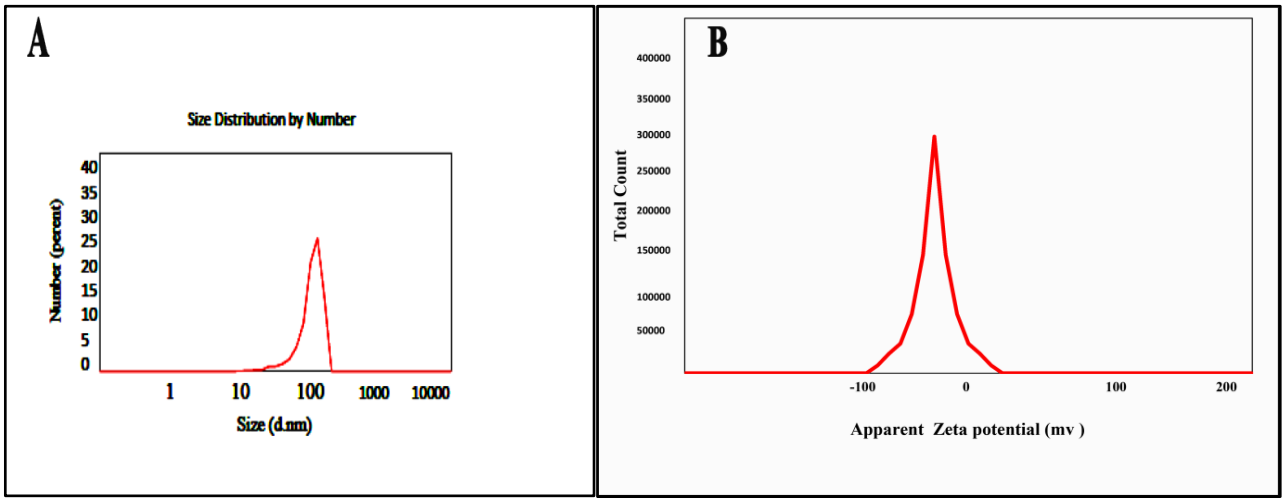

Figure 3: The hydrodynamic size and zeta potential of SiNPs synthesized using green methods in DMEM at 24 h.(A). DLS (nm) (B). Zeta potential (mV).

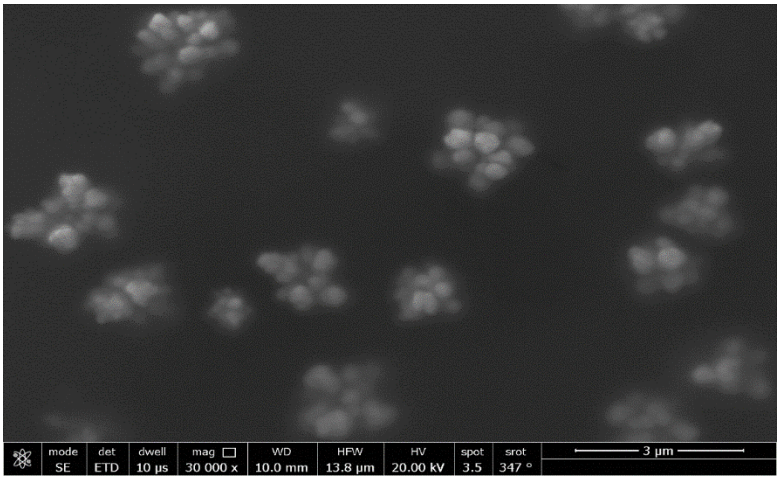

Figure 4: SEM image of silica nanoparticles synthesized using green methods

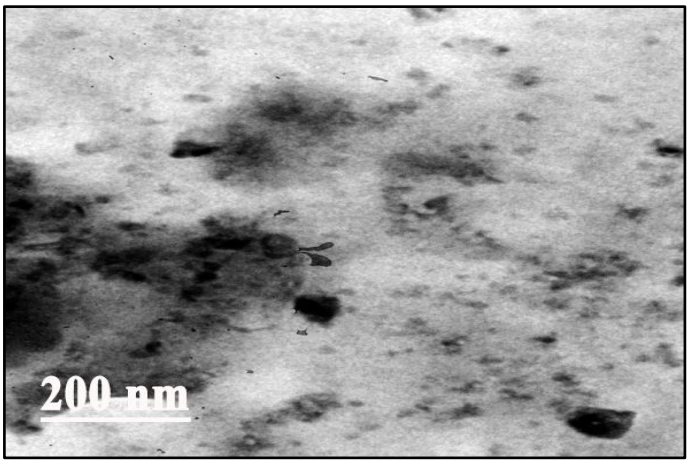

Figure 5: TEM image of silica nanoparticles synthesized using green methods

Cell viability assessment

MTT test is considered to be one of the most effective techniques to measure the cytotoxicity of the silica nanoparticles. As its being displayed in Figure 5, after determination of cell viability of A549 cells, the cells were reduced from 100% at concentration of 0.5 µg/ml to less than 10% Si-NPs after being treated with 100 µg/ml of Si-NPs for 24 hour.

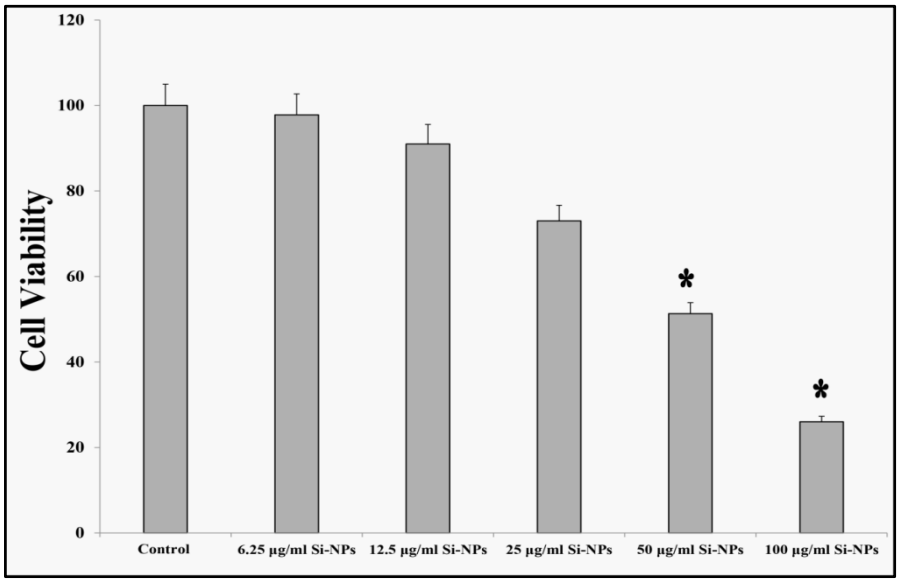

Figure 6: cell viability of A549 cell after treatment with different concentrations silica nanoparticles synthesized using green methods for 24 hours.

DNA content analysis

The cells can be arrest at different phase during the cell cycle because of the generation of reactive oxygen species as well as DNA damage. After 24 h treatment A549 with silica nanoparticles, the cell cycle phase was evaluated by using flow cytometry with propidium iodide (PI) staining. As shown in figure 6, Si-NPs Treatment enhanced the accumulation of the A549 cells at the S phase significantly ($P<0.05$) compared with the control. The percentages of the cells at S increase significantly ($P<0.05$) with increasing silica nanoparticles concentration. The growth of the A549 treated with 100 µg/ml silica nanoparticles was about 54.82, 8.13, and 37.28.16% at G0/1, G2/M, and S, respectively, in comparing to the negative control cells, in which the growth values were about 62.03, 10.39, and 27.58 % at G0/1, G2/M, and S, respectively, which means that the cell cycle arrest at S phase .

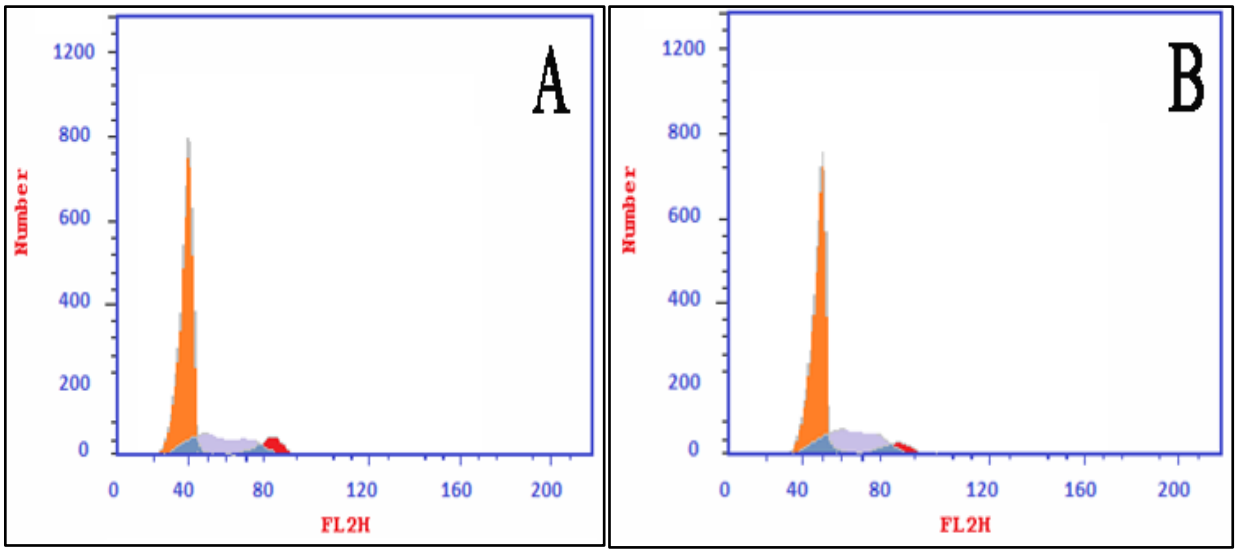

Figure 7: DNA content analysis A549 cell line treated with of silica nanoparticles.

a) Non-treated cell line
b) Cell line treated with 50 µg/ml of silica nanoparticles

A549 cells are induced to apoptosis by silica nanoparticles

silica nanoparticles induced apoptosis in cells has been analyzed by the flow cytometry through using Annexin V-FITC/PI staining as figures 7 (A,B) showed. The percentage of the apoptotic cells which include both early and late apoptotic cells have augmented by increasing silica nanoparticles concentration from 1.78 to 26.39 %, respectively.

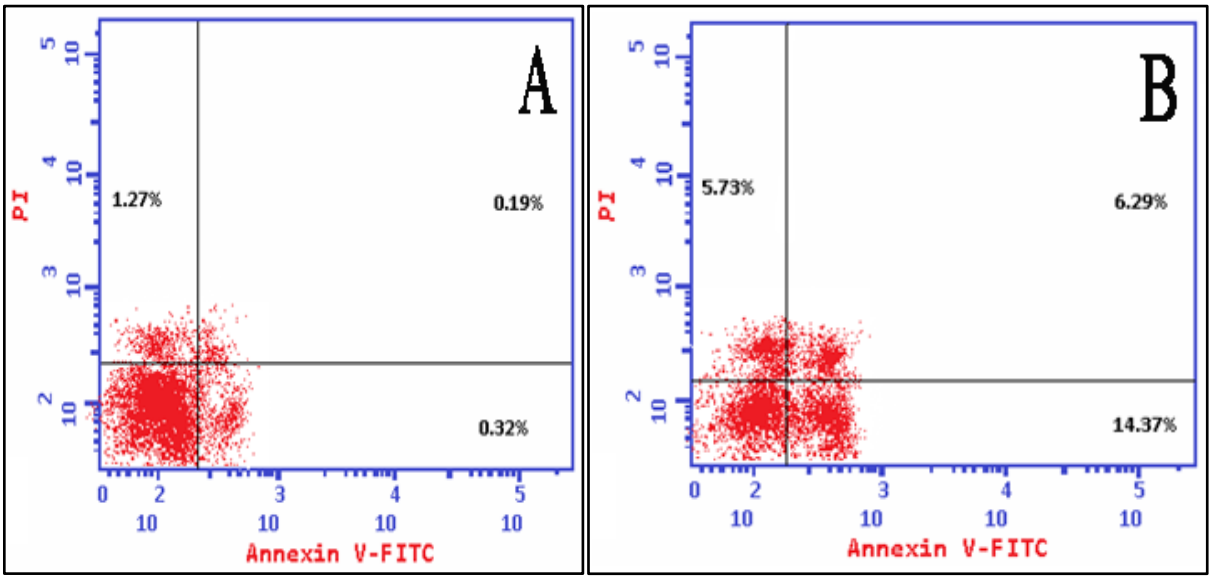

Figure 8: Apoptosis detection using Annexin V-FITC/PI staining protocol.

a) Non-treated cell line
b) Cell line treated with 50 µg/ml of silica nanoparticles

Quantitative RT-PCR

The levels of apoptotic genes (LC3, Beclin 1) those found in A549 cell were evaluated through silica nanoparticles treatment to the cell at a concentration 100 µg/ml for 24 h. The result disclosed that Si-NPs altered the expression of apoptotic genes in the cells. The assessment of mRNA expression levels of autophagic genes LC3 (Figure 8A), beclin-1 (Figures 8B,) were significantly unregulated.

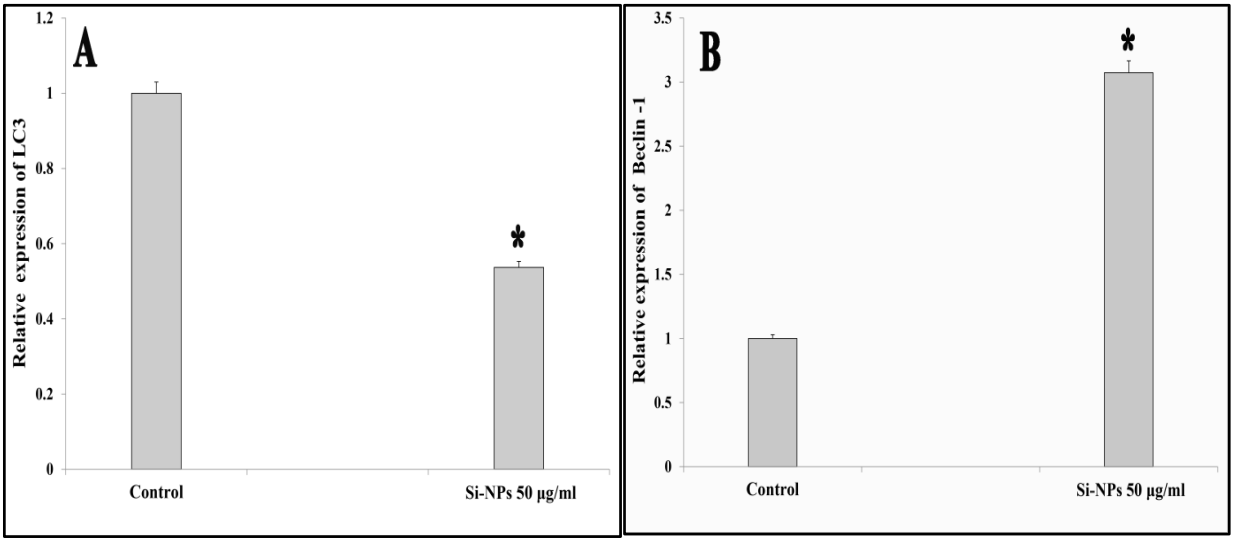

Figure 9: The figures are displaying the measurement of mRNA levels using Quantitative real-time PCR after exposure to concentration of 50 µg/ml of Si-NPs for 24 hour. *Statistically significant difference as in comparing to the controls (P, 0.05 for each). (A) LC3 (B) Beclin1.

Oxidative stress and antioxidant biomarkers

The MDA assay is consider as lipid peroxidation biomarker, which refers to oxidative stress. Figure 10 a shows a significant increase in oxidative stress mediators. MDA concentrations were reduced two-fold when compared to the negative control. The concentration of MDA was increases from 3.4 nmol/ml at a concentration of 50 µg/ml silica nanoparticles, as compared with the negative control. Also, silica nanoparticles increase the concentration of nitric oxide as antioxidant marker with three fold as compared with negative control. The concentration of NO was increases to 37 µmol/ml at a concentration of 50 µg/ml silica nanoparticles.

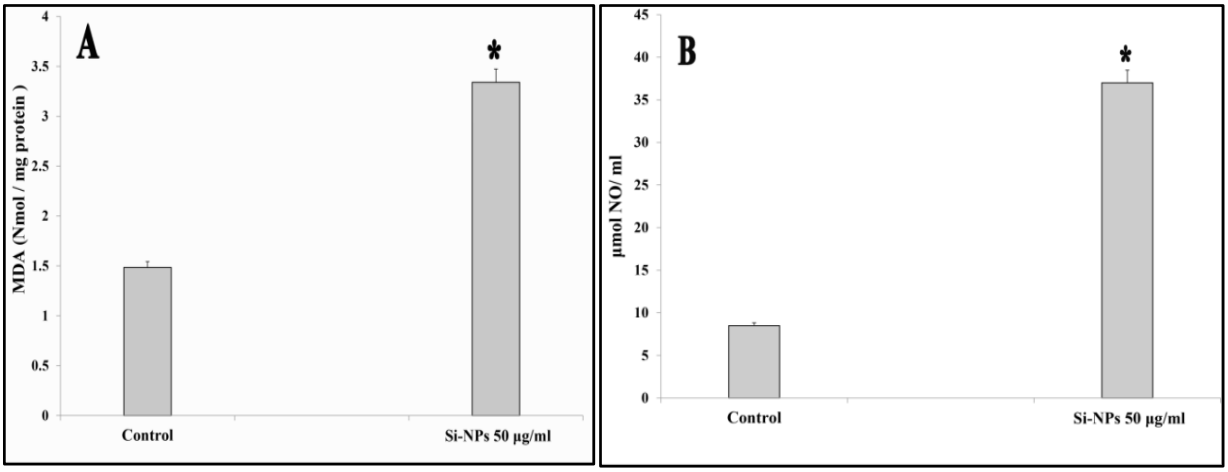

Figure 10: Oxidative and ant oxidative stress markers of human lung adenocarcinoma A549 cells after treated with 50 µg/mL Si-NPs. * Statistically significant difference when compared to the controls (P > 0.05 for each). (A) MDA (B) NO.

Caspase-3 activity assay

Caspase-3 is considered to be the executioner caspase and is activated by other caspases as 8, 9 and 10 as a result to the apoptotic events. Figure 11 showed that any increase in the silica nanoparticles concentraion will cause increasing in the caspase 3 enzyme activitiy to be 1.2 at a concentration of 50 µg/ml as compared to negative control. The data validate that silica nanoparticles activates the caspase 3 activity in a concentration-dependent manner.

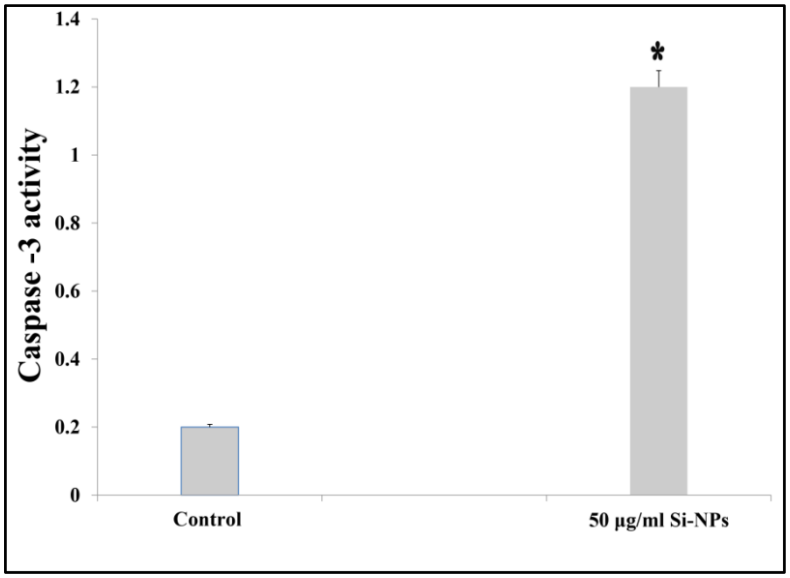

Figure 11: Determination of caspase-3 activity of silica nanoparticles. Statistically, we can notice a significant difference when compared to the controls (P> 0.05 for each).

Immunohistochemistry

Weaker Beclin 1 was immunohistochemically observed in A549 as silica nanoparticle interact with lung as showed in figure 12 b as compared with negative control (Figure 12 a).

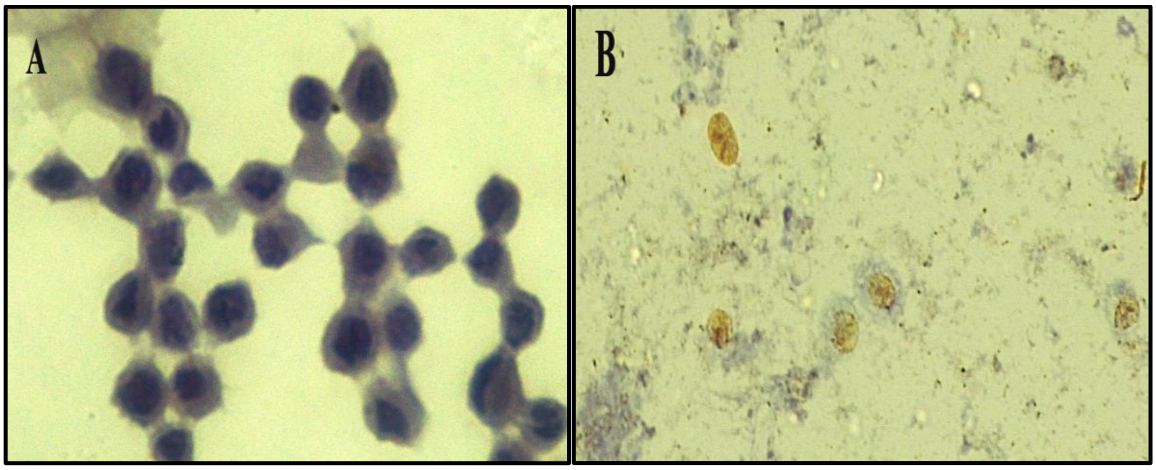

Figure 12: The effect of Becn1 expression immunoreactivity by silica nanoparticles on A549 cell line according to immunohistochemistry

a) Non-treated cell line
b) Cell line treated with 50 μg/ml of silica nanoparticles

Ultrastructure analysis

Visualization via transmission electron microscope of A549 cells those treated with silica nanoparticles at variety of concentrations revealed the typical characteristics of autophagosome accumulation associated with apoptotic cell stages: In the normal control cell (non-treated cell), there observed a cell with a normal subcellular organelles morphology with a few autophagic vacuoles (Figure.13A).While a number of autophagosomes and single-membrane autolysosomes was present as Si-NPs treated at concentration 25 μg/ml, as figure13 B showed. Furthermore, autophagosomes engulfed particle aggregates, damaged mitochondria, and misfolded proteins were also observed as figure 13 B displayed. Consequently, the morphological state revealed that the cells were rounded up with vanished cytoplasm. Furthermore, when the concentration ramped up to 50 μg/ml; there were several alterations in appearance as a result of chromatin condensation at the nuclear periphery and mitochondria tend to be conserved till secondary necrosis is being processed throughout treatment as it has been shown in figure 13 C.

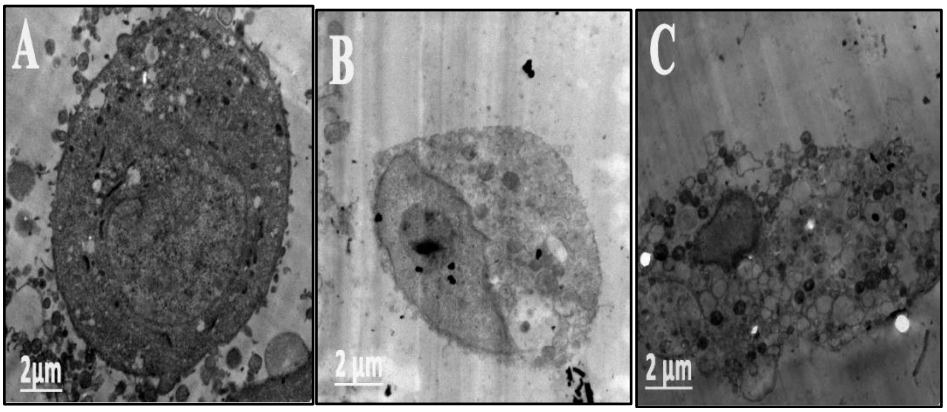

Figure 13: Images those created through transmission electron microscope which revealed A549 cells upon exposure to two concentrations of Si-NPs which are 25 and 50 mg/ml for nearly 24 hour. (A) Control. (B) Cell treated with 25 μg/ml of Si-NPs for 24 hour. (C) Treated cell with to 50 μg/ml of Si-NPs for 24 hour.

Discussion:

Globally, lung adenocarcinoma cancer is the main cause of death for men and women, especially non-small cell lung carcinoma that is considered responsible for nearly more than eighty-five percent of deaths. Many reports focus on the importance of autophagy as well as apoptosis mechanisms to the improvement of the novel therapy activity. Previous articles report that the activity of the metal nanoparticles induces autophagy [20]. Autophagy activation has occurred depending on the type of stress and the cellular microenvironment [21]. Also, autophagy may destroy or protect the cell [22–23]. It depends on the concentration of the metal nanoparticles; at high concentrations, metal nanoparticles can induce autophagy-dependent differentiation or autophagy-associated apoptosis [24]. Autophagy can induce apoptosis through activation of caspases, interaction with mediators of apoptotic pathways like the BCL2 family, or autophagy-dependent degradation of cytotoxic and aggregated proteins [25]. Furthermore, autophagy is related to associate self-digestive processes that can alter the morphological changes linked to differentiation (disappearance of mitochondria and/or nuclei) and cell survival during differentiation [26]. Beclin 1 has multiple roles in autophagy and apoptosis. Also, it is associated with vacuolar sorting protein 34 (PIK3C3/VPS34). This minimal unit is recruiting Multiple BECN1-interacting proteins, involving ATG14/Barkor (a BECN1-associated autophagy-related key regulator) [27]. The main mechanism by which BECN1 is associated with apoptosis and autophagy is by targeting post-translational modifications (PTMs), JNK1 or ERK1/2 mediated phosphorylation of BCL2 as a response to starvation, which result in dissemblance of the BECN1-BCL2 from each other [28]. Silica nanoparticles are one of the popular nanometals, which are listed as the top five materials in production due to their physicochemical properties. They are used in many biotechnological and biomedical fields [29]. Previous studies confirmed that silica nanoparticles successfully generate excess ROS, which may cause the following effects: DNA damage, cell cycle arrest, apoptosis, autophagy, and cell death [30–33]. Moreover, oxidative stress is considered a central regulator of autophagy; in other words, autophagy dysfunction was recently proposed as a potential toxic mechanism of nanomaterials [34]. In this work, silica nanoparticles were synthesized using a biological approach by the fungal *Aspergillus niger* as a reducing agent under aerobic conditions at pH 6.2 (weak acid medium). Consequently, silica nanoparticles were characterized using different tools such as FTIR, XRD, DLS, SEM, and TEM. The physicochemical data confirmed the formation of silica nanoparticles with a diameter of 35 nm. Also, in this work, the silica nanoparticles investigated the autophagy related to the apoptosis mechanism against lung adenocarcinoma A549 through different tools such as apoptosis, DNA content, caspase 3 assays, oxidative and ant-oxidative stress markers, RT-PCR, immunohistochemistry, and transmission electron microscopy. The results revealed that silica nanoparticles activated apoptosis with 26.39% and arrested the cell cycle at S phase due to an increase in the percentage of cells at S with 10 percent as compared with the negative control. Furthermore, the caspase 3 assay indicated that the activity of silica nanoparticles to induce apoptosis throughout the caspase cascades was evaluated by inducing oxidative stress (MDA), which is considered a lipid peroxidation marker. The rt-Pcr results showed down-regulation of LC3, while beclin 1 showed overexpression. Both LC3 and beclin 1 are autophagic genes that regulate the autophagy process. The immunohistochemistry showed showed weaker Beclin 1. Transmission electron microscopy showed autophagosomes that are considered the benchmark for autophagy studies; the number of double-membrane autophagosomes and single-membrane autolysosomes was obviously observed in SiNP-treated A549. The lysosome ultrastructures, as shown in Figure 13, accumulate in lysosomes, which causes the swelling of lysosomes. Moreover, some silica nanoparticles were scattered in the cytoplasm of nanoparticle-treated cells. Previous studies have shown the effect of metal nanoparticles to induce autophagy, such as zinc oxide nanoparticles. Bai et al. (2017) demonstrated the ability of nanoparticles those fabricated in the zinc oxide form to stimulate autophagy in ovarian cells of human through creating reactive oxygen species (ROS), leading to oxidative stress [35]. Also, Moosavi and colleagues (2016) emphasized that the photodynamic therapy (PDT) of nitrogen-doped titanium nanoparticles

induced autophagy through the generation of reactive oxygen species (ROS) [24]. Finally, these results indicate that the cytotoxicity of SiNPs may involve the autophagic pathway in A549 cells.

Conclusion:

In this work, silica nanoparticles were synthesized using a biological approach by the fungal *Aspergillus niger* as a reducing agent under aerobic conditions at pH 6.2 (weak acid medium). Consequently, silica nanoparticles were characterized using different tools such as FTIR,XRD, DLS, SEM, and TEM. The physicochemical data confirmed the formation of silica nanoparticles with a diameter of 35 nm. Also, in this work, the silica nanoparticles investigated the autophagy related to the apoptosis mechanism against lung adenocarcinoma A549 through different tools such as apoptosis, DNA content, caspase 3 assays, oxidative and ant-oxidative stress markers, RT-PCR, immunohistochemistry, and transmission electron microscopy. The results revealed that silica nanoparticles activated apoptosis with 26.39% and arrested the cell cycle at S phase due to an increase in the percentage of cells at S with 10 percent as compared with the negative control. Furthermore, the caspase 3 assay indicated that the activity of silica nanoparticles to induce apoptosis throughout the caspase cascades was evaluated by inducing oxidative stress (MDA), which is considered a lipid peroxidation marker. The rt-Pcr results showed down-regulation of LC3, while beclin 1 showed overexpression. Both LC3 and beclin 1 are autophagic genes that regulate the autophagy process. The immunohistochemistry showed a weaker Beclin 1. Transmission electron microscopy showed autophagosomes that are considered the benchmark for autophagy studies; the number of double-membrane autophagosomes and single-membrane autolysosomes was obviously observed in SiNP-treated A549. Finally, these results indicate that the cytotoxicity of SiNPs may involve the autophagic pathway in A549 cells.

Data Access Statement:

All of the original contributions those existed in the study are noted in the article; any additional inquiries can be asked to the corresponding author.

Acknowledgments:

The researchers would like to acknowledge the Deanship of scientific research at Taif University for providing facilities and labs for performing the current experimental work.

Conflicts of Interest (COI):

All of the authors clarify that the research has been completed without any potential conflict of interest.

Author contributions:

Conceptualization: Fawziah A. Al-Salmi; formal analysis: Fawziah A. Al-Salmi funding acquisition: Fawziah A. Al-Salmi, : investigation: Fawziah A. Al-Salmi; investigation, Fawziah A. Al-Salmi project administration: Fawziah A. Al-Salmi; Resource: Fawziah A. Al-Salmi, ; supervision: Fawziah A. Al-Salmi; Validation: Fawziah A. Al-Salmi visualization: Fawziah A. Al-Salmi ; writing original draft: Fawziah A. Al-Salmi: writing -review edition; Fawziah A. Al-Salmi. The author approved the final version of the manuscript.

References:

1. Siegel, R. L., Miller, K. D., & Jemal, A. (2018). Cancer statistics, 2018. *CA: a cancer journal for clinicians*, *68*(1), 7-30.
2. Baker, S., Dahele, M., Lagerwaard, F. J., & Senan, S. (2016). A critical review of recent developments in radiotherapy for non-small cell lung cancer. *Radiation oncology*, *11*, 1-14.
3. Rich, J. N. (2007). Cancer stem cells in radiation resistance. *Cancer research*, *67*(19), 8980-8984.

4. Li, J., Liu, G., Li, L., Yao, Z., & Huang, J. (2020). Research progress on the effect of autophagy-lysosomal pathway on tumor drug resistance. *Experimental cell research*, *389*(2), 111925.
5. Hou, G., Bai, Y., Jia, A., Ren, Y., Wang, Y., Lu, J., ... & Lu, Z. (2020). Inhibition of autophagy improves resistance and enhances sensitivity of gastric cancer cells to cisplatin. *Canadian Journal of Physiology and Pharmacology*, *98*(7), 449-458.
6. Kang, R., Zeh, H., Lotze, M., & Tang, D. (2020). The multifaceted effects of autophagy on the tumor microenvironment. *Tumor Microenvironment: Recent Advances*, 99-114.
7. Mizushima N. The exponential growth of autophagy-related research:From the humble yeast to the Nobel Prize. FEBS Lett 2017; 591(5):681–9.
8. Ozpolat B, Benbrook DM. Targeting autophagy in cancer management strategies and developments. Cancer Manag Res 2015; 7: 291–9.
9. Vega-Rubín-de-Celis, S. (2019). The role of Beclin 1-dependent autophagy in cancer. *Biology*, *9*(1), 4.
10. Mele L, Del Vecchio V, Liccardo D, Prisco C, Schwerdtfeger M, Robinson N, et al. The role of autophagy in resistance to targeted therapies. Cancer Treat Rev 2020; 88: 102043.
11. Li X, He S, Ma B. Autophagy and autophagy-related proteins in cancer. Mol Cancer 2020; 19(1): 12.
12. Hassan A, Elebeedy D, Matar ER, Fahmy Mohamed Elsayed A and Abd El Maksoud AI (2021) Investigation of Angiogenesis and Wound Healing Potential Mechanisms of Zinc Oxide Nanorods. Front. Pharmacol. 12:661217. doi: 10.3389/fphar.2021.661217.
13. Hassan, A., AL-Salmi, F. A., Saleh, M. A., Sabatier, J. M., Alatawi, F. A., Alenezi, M. A., ... & Sharaf, E. M. (2023). Inhibition Mechanism of Methicillin-Resistant Staphylococcus aureus by Zinc Oxide Nanorods via Suppresses Penicillin-Binding Protein 2a. ACS Omega.
14. Hassan A, Al-Salmi FA,Abuamara TMM, Matar ER, Amer ME,Fayed EMM, Hablas MGA, Mohammed TS, Ali HE,Abd EL-fattah FM, Abd Elhay WM,Zoair MA, Mohamed AF, Sharaf EM, Dessoky ES, Alharthi F, Althagafi HAEand Abd El Maksoud AI (2022)Ultrastructural analysis of zinc oxidenanospheres enhances anti-tumor efficacy against Hepatoma. Front. Oncol. 12:933750.doi: 10.3389/fonc.2022.933750.
15. Sharaf EM, Hassan A, AL-Salmi FA, Albalwe FM, Albalawi HMR, Darwish DB and Fayad E (2022) Synergistic antibacterial activity of compact silver/magnetite core-shell nanoparticles core shell against Gram-negative foodborne pathogens. Front. Microbiol. 13:929491. doi: 10.3389/fmicb.2022.929491
16. Liu, J.; Li, C.; Li, F. Fluorescence turn-on chemodosimeter- functionalized mesoporous silica nanoparticles and their application in cell imaging. *J. Mater. Chem.* **2011,** *21*,7175-7181.
17. Ehlert, N.; Mueller, P.; Stieve, M.; Lenarz, T.; Behrens, P. Mesoporous silica films as a novel biomaterial: applications in the middle ear. *Chem. Soc. Rev.* **2013,** *42*, 3847-3861.
18. Salinas, A. J., Esbrit P, Vallet-Regi M. A tissue engineering approach based on the use of bioceramics for bone repair. *Biomater. Sci.* **2013,** *1*, 40-50.
19. Liong, M.; Lu. J.; Kovochich, M.; Xia, T.; Ruehm, S.G.; Nel, A.E.; Tamanoi, F.; Zink,J.I. Multifunctional inorganic nanoparticles for imaging, targeting, and drug delivery.*ACS Nano* **2008,** *2*, 889-896.
20. Peynshaert, K. et al. Exploiting intrinsic nanoparticle toxicity: the pros and cons of nanoparticle-induced autophagy in biomedical research. Chemical reviews 114, 7581–7609 (2014).
21. Popp, L. & Segatori, L. Differential autophagic responses to nano-sized materials. Current opinion in biotechnology 36, 129–136 (2015).
22. Tedja, R., Lim, M., Amal, R. & Marquis, C. Effects of serum adsorption on cellular uptake profile and consequent impact of titanium dioxide nanoparticles on human lung cell lines. ACS nano 6, 4083–4093 (2012).

23. Lopes, V. R. et al. Dose-dependent autophagic effect of titanium dioxide nanoparticles in human HaCaT cells at non-cytotoxic levels. Journal of nanobiotechnology 14, 1 (2016).
24. Moosavi, M. A. et al. Photodynamic N-TiO2 Nanoparticle Treatment Induces Controlled ROS-mediated Autophagy and Terminal Differentiation of Leukemia Cells. Sci. Rep. 6, 34413; doi: 10.1038/srep34413 (2016).
25. Rubinstein, A. D. & Kimchi, A. Life in the balance–a mechanistic view of the crosstalk between autophagy and apoptosis. Journal of cell science 125, 5259–5268 (2012).
26. Cao, Y. et al. Loss of autophagy leads to failure in megakaryopoiesis, megakaryocyte differentiation, and thrombopoiesis in mice.Experimental hematology 43, 488–494 (2015).
27. Song, X., Zhu, S., Chen, P., Hou, W., Wen, Q., Liu, J., et al. (2018). AMPK mediated BECN1 phosphorylation promotes ferroptosis by directly blockingSystem Xc(-) activity. Curr. Biol. 28, 2388–2399.e5. doi: 10.1016/j.cub.2018.05.094.
28. Menon MB and Dhamija S (2018) Beclin 1 Phosphorylation – at the Center of Autophagy Regulation. Front. Cell Dev. Biol. 6:137. doi: 10.3389/fcell.2018.00137.
29. Wang Y, Zhao Q, Han N, et al. Mesoporous silica nanoparticles in drug delivery and biomedical applications. Nanomedicine. 2015; 11(2):313–327.
30. Niu M, Zhong H, Shao H, et al. Shape-dependent genotoxicity of mesoporous silica nanoparticles and cellular mechanisms. J Nanosci Nanotechnol. 2016;16(3):2313–2318.
31. Lin YH, Chen YP, Liu TP, et al. Approach to deliver two antioxidant enzymes with mesoporous silica nanoparticles into cells. ACS Appl Mater Interfaces. 2016;8(28):17944–17954.
32. .Xi C, Zhou J, Du S, Peng S. Autophagy upregulation promotes macrophages to escape mesoporous silica nanoparticle (MSN)-induced NF-kappaB-dependent inflammation. Inflamm Res. 2016;65(4):325–341.
33. Saito T, Ichimura Y, Taguchi K, et al. P62/Sqstm1 promotes malignancy of HCV-positive hepatocellular carcinoma through Nrf2-dependent metabolic reprogramming. Nat Commun. 2016;7:12030.
34. Stern ST, Adiseshaiah PP, Crist RM. Autophagy and lysosomal dysfunction as emerging mechanisms of nanomaterial toxicity. Part Fibre Toxicol. 2012;9:20.
35. Bai, D. P., Zhang, X. F., Zhang, G. L., Huang, Y. F., & Gurunathan, S. (2017). Zinc oxide nanoparticles induce apoptosis and autophagy in human ovarian cancer cells. *International journal of nanomedicine*, *12*, 6521.